Structure and Dynamics of Liquid Diphenyl Carbonate Investigated by Molecular Dynamics Simulations

Hendrik Meyer,* Oliver Hahn, and Florian Müller-Plathe

Max-Planck-Institut für Polymerforschung, 55021 Mainz, Germany

Received: May 26, 1999; In Final Form: September 16, 1999

We study liquid diphenyl carbonate (DPC) with molecular dynamics simulations in the temperature range from 350 to 600 K. The diffusion behavior as well as structural and relaxation properties of this complex liquid are analyzed in detail. To this end, an all-atom force field is developed for DPC. We studied two sets of partial charges and the influence of the torsion barrier at the carbonate group. We discuss radial distribution functions, orientation distribution functions, and orientation correlation functions of subgroups of the molecule. The flip frequencies of the dihedral angles of the phenyl rings and of the carbonate group are also considered. The internal flexibility and the nonspherical form of the molecule highly improve the diffusion process, whereas the height of the carbonate group torsion barrier is not a crucial parameter.

I. Introduction

Diphenyl carbonate (DPC) is the main building block of the polycarbonate family. Since their first synthesis in 1955, polycarbonates have become industrially very important polymers, mainly because they combine several desirable properties, such as electrical insulation, high heat of distortion, transparency, and impact resistance.[1] Consequently, considerable experimental and theoretical research has been carried out to understand the reason for this unique combination of material properties of polycarbonates. In particular, for the purpose of material design it would be highly desirable to be able to link the molecular structure and dynamics to these macroscopic quantities.

In this respect, molecular dynamics (MD) simulations provide a unique tool to investigate these materials on the atomistic level. In the present piece of work, we address DPC, which is the common part of several important polycarbonate modifications such as bisphenol-A−polycarbonate and trimethylcyclohexane−polycarbonate. We, therefore, use simulations of liquid DPC to parametrize an all-atom force field that can be merged with already existing force fields to obtain a reliable set of force field parameters for the polycarbonate family.[2] Existing force fields for polycarbonates always consider DPC as a building block, but there are no MD studies of the DPC melt itself. Existing force fields mostly rely on quantum calculations for parts of the DPC molecule.[3,4] Improved computational power allows us to optimize the whole DPC molecule at the HF6-311G** level with higher precision consistent with recent independent density functional theory (DFT) calculations.[5,6]

Furthermore, there is considerable dispute in the literature on glassy polycarbonates[6−8] as to whether the most important mechanism for the chain motion is conformational transitions (trans−trans → cis−trans) at the carbonate group or phenylene ring flips. Since it is impossible to study the diffusion of polycarbonate chains in a melt by means of an atomistic MD,[9] the simulation of liquid DPC seems appealing to gain insight into the interplay between conformational transitions at the carbonate group and diffusion. In more general terms, this case study should be interesting on its own, since it allows the comparison of diffusion dynamics of strongly anisotropic molecules with internal degrees of freedom with that of rigid, nearly spherical molecules.

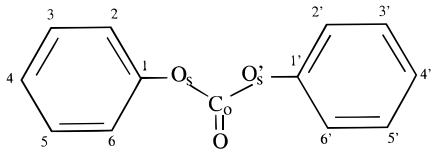

Figure 1. Diphenyl carbonate (DPC) with the atom names used in Table 1.

II. Force Field and Simulation Details

We report in this article extensive molecular dynamics (MD) simulations of liquid diphenyl carbonate (DPC) with an all-atom force field using the MD code YASP.[10] It allows for full flexibility of torsions and bond angles. Only bond lengths are kept constant. Compatible force fields for liquid phenol and benzene have already been developed and are described in the literature.[11] A study of polycarbonates with a force field based on the parameters of this article will be published elsewhere.[2]

A. The Force Field. The form of the force field employed in this work, used to describe the potential energy experienced both within and between diphenyl carbonate molecules (see Figure 1), is given by

$$E_{\mathrm{pot}} = \sum_{\text{angles}} \frac{1}{2} k_\theta (\theta - \theta_0)^2 + \sum_{\text{dihedrals}} \frac{1}{2} k_\tau [1 - \cos n(\tau - \tau_0)] + \sum_{\text{h-dihedrals}} \frac{1}{2} k_\delta (\delta - \delta_0)^2 + \sum_{i<j} 4\epsilon_{ij} \left[\left(\frac{\sigma_{ij}}{r_{ij}} \right)^{12} - \left(\frac{\sigma_{ij}}{r_{ij}} \right)^{6} \right] + \sum_{i<j} \frac{q_i q_j}{4\pi\epsilon_0} \left(\frac{1}{r_{ij}} + \frac{\epsilon_{\mathrm{RF}} - 1}{2\epsilon_{\mathrm{RF}} + 1} \frac{r_{ij}^2}{r_{\mathrm{cutoff}}^3} \right) \quad (1)$$

where the total potential energy, E_{pot}, has contributions from bond angle bending (k_θ, θ_0), dihedral angle deformation about the C_1-O_s (aromatic carbon−ester oxygen) and C_o-O_s (carbon-

* Corresponding author. E-mail: hmeyer@mpip-mainz.mpg.de.

10.1021/jp991733c CCC: $18.00
Published on Web 11/04/1999

TABLE 1: Potential Energy Function Parameters for Model Diphenyl Carbonate[a]

atom	ϵ/kJ mol^{-1}	σ/nm	$q_i^{FF(1)}$/e	$q_i^{FF(2)}$/e
O_s	0.712	0.300	−0.35	−0.308
C_o	0.360	0.340	0.65	0.63
O	0.880	0.296	−0.30	−0.378
C_1	0.294	0.355	0.33	0.294
$C_{2,6}$	0.294	0.355	−0.22	−0.21
$C_{3,5}$	0.294	0.355	−0.04	−0.042
C_4	0.294	0.355	−0.125	−0.133
$H_{2,6}$	0.126	0.242	0.12	0.126
$H_{3,5}$	0.126	0.242	0.08	0.091
H_4	0.126	0.242	0.09	0.091

bond constraint	distance/nm
C_o-O	0.118
C_o-O_s	0.132
O_s-C_1	0.139
C−C	0.139
C−H	0.108

bond angle	θ_o/deg	k_θ/kJ mol^{-1} rad^{-2}
$O_s-C_o-O_s$	108.0	418.8
O_s-C_o-O	126.0	418.8
C_1-Os-C_o	121.4	418.8
$C_{2,6}-C_1-C_s$	120.0	418.8
C−C−C	120.0	376.6
C−C−H	120.0	418.8

torsion	τ_o/deg	$k_\tau^{FF(1)}$/kJ mol^{-1}	n	$k_\tau^{FF(2)}$/kJ mol^{-1}
$O_s-C_o-O_s-C_1$	180	22.0	2	15.0
$O-C_o-O_s-C_1$	180	22.0	2	15.0
$O_s-C_o-O_s-C_1$	180	−	1	4.0
$C_o-O_s-C_1-C_{2,6}$	180[b]	1.5	2	1.5

harmonic dihedrals	δ_0/deg	k_δ/kJ mol^{-1}
C−C−C−C	0.0	167.4
$C_2-C_3-C_1-H_2$ [and equivalent]	0.0	167.4
$C_1-C_2-C_6-O_s$ [on C_1]	0.0	167.4
$C_o-O_s-O'_s-O$ [on C_o]	0.0	167.4

[a] For the naming of atoms see Figure 1. Two different sets of partial charges q_i and torsion potential barriers are given defining FF(1) and FF(2) (see text). [b] Note that the effective minimum of this dihedral is stabilized by the nonbonded interactions at ±90° giving rise to too high a barrier; the purpose of this torsional term is to decrease the effective barrier.

ate carbon−ester oxygen) bonds (k_τ, τ_0), harmonic dihedral bending (k_δ, δ_0), and nonbonded interactions in the form of Lennard-Jones (ϵ_{ij}, σ_{ij}) and point-charge electrostatics (q_i, q_j, ϵ_{RF}). The Kirkwood approximation for a reaction field with dielectric constant, ϵ_{RF}, is used to model the long-range interaction of a dipole with its surroundings. The terms in parentheses denote the parameters that define the force field.

All parameters associated with the phenyl ring (except charges) were taken from the benzene model of Jorgensen and Severance.[12] Lennard-Jones parameters for the carbonate group are taken from the AMBER force field.[13] Nonbonded interactions are excluded between all atoms inside the phenyl rings and up to the third neighbor with atoms of the carbonate group. The main potential parameters to be determined were the partial charges for each atom and the torsional barrier about the C_1-O_s and C_o-O_s bonds. We finally performed simulations with two force fields FF(1) and FF(2) which differ in the partial charges and the torsional barrier at the carbonate group. Figure 1 describes the naming of atoms; Table 1 contains all force field parameters.

The partial charges have been determined from a fit of atomic point charges to the electrostatic potential (ESP) on the molecular surface, generated using DFT techniques, according to the Merz−Singh−Kollman scheme.[14,15] A first guess of charges determined from an ESP fit with the charge distribution calculated in B3LYP and an STO-3G basis set was used in FF-(1). This yielded already quite good results. Afterward, we repeated the ESP fit procedure with the charge distribution calculated in B3LYP and a 6-311G** basis set. This yielded charges which were much larger. To get a reasonable coincidence with the experimental density and heat of vaporization, these charges had to be rescaled by 70%. The resulting set of partial charges used in FF(2) are on the same order as the charges from FF(1), except the dipole moment at the carbonate group is slightly increased. Both sets of partial charges are given in Table 1.

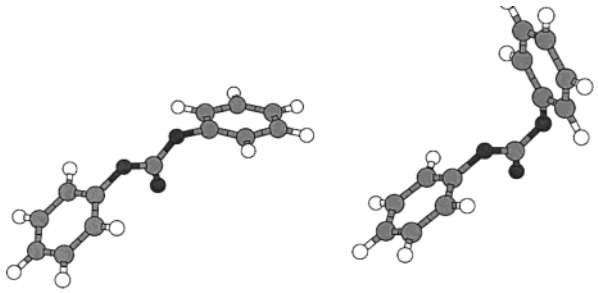

Figure 2. Diphenyl carbonate in a trans−trans conformation with minimum energy (left) and in the cis−trans conformation (right).

The rotational barriers were determined from Hartree−Fock (6-311G** basis set) and hybrid density functional theory (B3LYP, 6-311G** basis set) calculations in the gas phase. A minimum energy structure for DPC is shown in Figure 2. Bond lengths and angles are in good agreement with crystal structure data.[16] Equilibrium values for the dihedral angles at the carbonate group are about ±90° for dihedrals associated with the C_1-O_s bonds and 0° and 180° for dihedrals associated with the C_o-O_s bonds. The barrier to rotation about the C_1-O_s bonds for turning the phenyl rings is found to be quite low with 3.6 kJ/mol between the 0° and the 90° conformation. In fact, careful treatment of the whole DPC molecule at the level HF6-311G** yields two minimum energy conformations of the C_1-O_s phenyl ring torsion: At an angle of about 75° between the plane of the carbonate group and the plane of the two phenyl rings, the energy is lowered by less than 0.1 kJ/mol with respect to the 90° conformation. A second minimum is found when the two phenyl rings are turned by about 66° to different sides with respect to the carbonate group being 0.4 kJ/mol lower than the 90° conformation (this conformation is called *anti* in ref 6). As we are interested in liquid properties well above room temperature, these small energy differences can be neglected and we chose a symmetric potential having ±90° as the minimum energy position without correlations between the two phenyl rings.

The barrier to rotation about the C_o-O_s bonds was first calculated for dimethyl carbonate (DMC), supposing that the phenyl rings do not influence the carbonate group. This yields a value of ∼40 kJ mol^{-1} (16.0 k_BT at 298 K). In FF(1), we used a value of 44 kJ mol^{-1} for the torsional potential since the nonbonded parameters lower the energy at the maximum by about 4 kJ mol^{-1}. We repeated the quantum calculation with the whole DPC molecule. This shows that the approximation not considering the phenyl rings is not justified since there is a considerable delocalization of electrons from the phenyl rings to the carbonate group (this was also pointed out in ref 6). The barrier to rotation about the C_o-O_s bond is thus found to be about 26 kJ mol^{-1}; we used a value of 30 kJ mol^{-1} for the

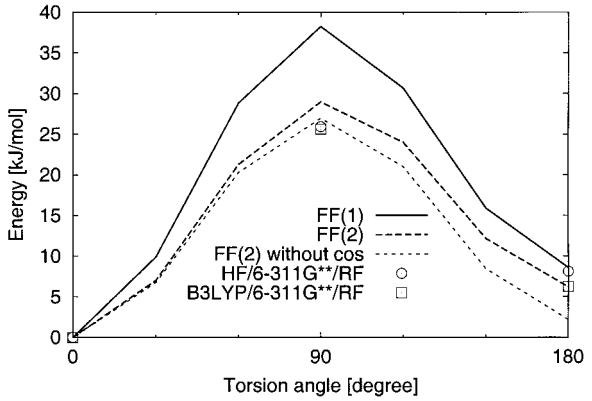

Figure 3. Energy barrier for rotation about the C_o-O_s carbonate bond. 0 corresponds to the trans−trans conformation, 180 to the cis−trans conformation. Points represent quantum calculations with the whole DPC molecule and an Onsager reaction field: ○, Hartree−Fock (HF) 6-311G** basis set; □, density functional theory (B3LYP) 6-311G** basis set. Lines represent the effective barrier with the force fields presented in this work.

torsional potential of the C_o-O_s bonds in FF(2). The effective potential barrier of both force fields is shown in Figure 3. In FF(1), the energy of the cis−trans conformation is about 8 kJ mol^{-1} higher than that of the trans−trans ground state conformation in agreement with calculations on DMC. Using the different partial charges of FF(2), the cis−trans conformation is only 2.2 kJ mol^{-1} above the trans−trans conformation. Quantum calculations (B3LYP, basis 6-311G**) with DPC yield 8.1 kJ mol^{-1} in vacuum and 6.2 kJ mol^{-1} with an Onsager reaction field calculation. We thus added a cosine potential with periodicity 1 and amplitude 4 kJ mol^{-1} to reach the energy difference of 6.2 kJ mol^{-1} between the trans−trans and the cis−trans conformations.

B. Simulation Details. All molecular dynamics simulations are performed using the YASP program.[10] Calculations were run at constant temperature T and constant pressure $p = 101.3$ kPa using Berendsen's thermostat and manostat[17] with isotropic pressure coupling, with coupling times of 0.2 ps (T) and 5 ps (p). Diphenyl carbonate consists of 26 atoms, and its size is approximately $1.2 \times 0.7 \times 0.5$ nm^3. Trial runs during force field parametrization (section II.A) were carried out with 64 molecules. Final production runs were performed with 216 molecules (5616 atoms). The resulting simulation box size was about (4.2 nm)^3. Periodic boundary conditions were used. Bond lengths were kept constant using the SHAKE algorithm.[18] The integration time step was 2 fs; configurations were sampled every 1 ps. The cutoff for nonbonded interactions was chosen to be 1.2 nm. The reaction field approximation was used with $\epsilon_{RF} = 3.5$, which is near the experimental value for polycarbonates of which DPC is a building block. For DPC itself, no dielectric constant was found.

Starting with a regular packing, a long equilibration run of about 1 ns was done at 393 K. During this equilibration, we used a lower value of the carbonate torsion barrier of 13.6 kJ/mol to enable the torsional states to find their equilibrium distribution (see also the discussion in section III.E). Then equilibration at each temperature was performed for about 0.5 ns with FF(1). Equilibration of temperature and density needed less than 0.1 ns, but conformational degrees of freedom, mainly the C_o-O_s torsions, needed more time to relax. Data were collected from production runs of up to 3 ns (see Table 2). Runs with FF(2) were started from a well-equilibrated configuration with FF(1), the first 200 ps being discarded for equilibration with the changed force field parameters.

TABLE 2: Physical Properties of Diphenyl Carbonate[a]

	T/K						
	350	393.15	400	450	500	573.15	600
time/ps FF(1)	3000	3000	1600	1400	1600	2000	1600
time/ps FF(2)			2000	1200		1200	
$\rho_{FF(1)}$	1111	1071	1065	1020	973	903	873
$\rho_{FF(2)}$			1069	1024		909	
ρ_{exp}		1074	1068	1025			
ΔH_{vap}, FF(l)	76.7	72.6	71.9	67.5	63.1	57.3	54.9
ΔH_{vap}, FF(2)			73.4	68.8		58.4	
$\Delta H_{vap,exp}$		74.0	73.2	68.2	64.4	59.8	
$D_{FF(1)}$	0.34	0.80	0.88	1.68	2.55	4.9	5.8
$D_{FF(2)}$			0.86	1.69		4.5	

[a] Units are density, ρ, kg m^{-3}; heat of vaporization, ΔH_{vap}, kJ mol^{-1}; diffusion coefficient, D, 10^{-5} cm^2 s^{-1}. "time" = length of trajectory used for averaging. Experimental sources: density, heat of vaporization from ref 19. Subscripts: FF(1), FF(2), simulation with force fields of this work; *exp*, experiment.

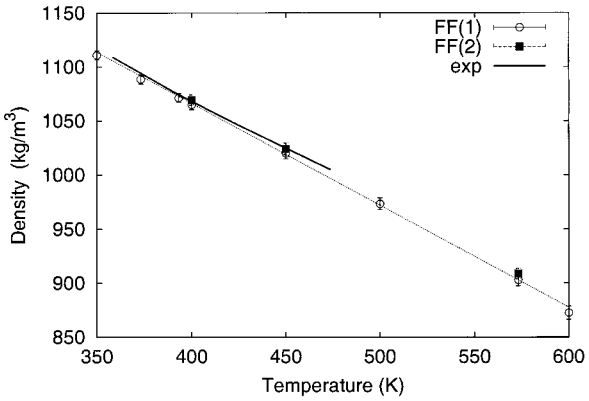

Figure 4. Diphenyl carbonate mass density. ○, force field FF(1); ■, force field FF(2); solid line, experiment;[19] the dashed line is a guide to the eye. Error bars represent the standard deviation for data collected during simulations.

III. Simulation Results

We now describe the results of the physical behavior of the DPC melt. Surprisingly, the physical results with the two force fields FF(1) and FF(2) are quite similar and most figures have been produced with data from FF(1). At the end of this section, the discussion of the influence of the torsion barrier at the carbonate group will lead to an understanding of these similarities. For future use, we recommend FF(2) unless there might be new experimental insights.

A. Thermodynamic Properties. Density and heat of vaporization are the two only quantities for which experimental data are available.[19] They have been used to optimize the nonbonded parameters of the force field. The temperature dependence of these two quantities is shown in Figures 4 and 5. The density of diphenyl carbonate in Figure 4 fits quite well the available experimental data which are about 0.5% larger than the simulated density in FF(1). With FF(2) the coincidence is even better. From

$$\sigma = \frac{1}{V}\frac{\partial V}{\partial T} = \rho\frac{\partial(1/\rho)}{\partial T} \tag{2}$$

we determine an isobaric thermal expansion coefficient of $\alpha = 0.9 \times 10^{-3}$ K^{-1} at 400 K.

The heat of vaporization is shown in Figure 5. The continuous line has been obtained using the Clausius−Clapeyron equation with the experimental vapor pressure curve[19] which fits very well the polynomial $\ln P^{vap} = 20.6 - 3.48 \times 10^3/T - 1.06 \times$

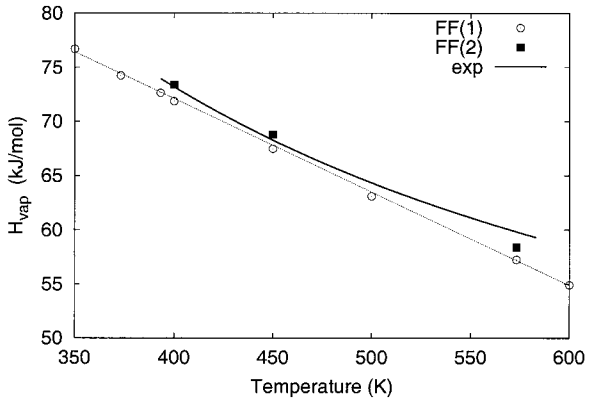

Figure 5. Diphenyl carbonate heat of vaporization. ○, force field FF-(1); ■, force field FF(2); solid line, calculated from the slope of experimental vapor pressure data;[19] the dashed line is meant as a guide to the eye obtained by linear fit through the points of FF(1). Statistical errors are smaller than the symbols.

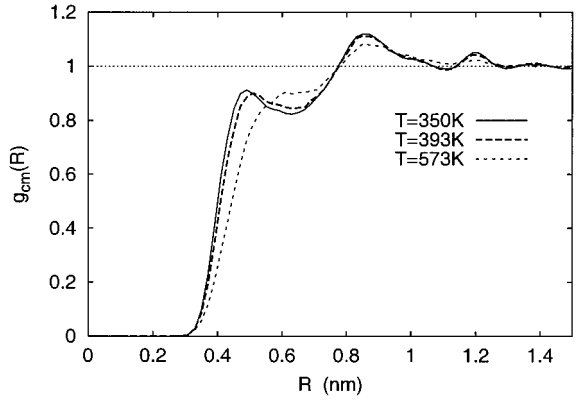

Figure 6. Radial distribution function for the centers of mass. Integration from 0 to 0.53 (0.56) nm yields 1 neighboring molecule; from 0 to 1.0 (1.05) nm yields 12 neighboring molecules at 393 K (573 K).

$10^6/T^2$. The simulation values are obtained from the intermolecular interaction energy $E_{pot,nonb}$ plus the work of volume expansion RT (R being the universal gas constant):

$$\Delta H_{vap} = -E_{pot,nonb} + RT \tag{3}$$

This simulation value is systematically smaller than that derived from experiment, by about 1% at 450 K and up to 4% at 573 K. With FF(2), the values are slightly larger than in FF(1), leading to a better coincidence with experimental values: the values are less than 1% larger than the experimental value at 400 and 450 K; the largest deviation is found at 573 K with 2.4% below the experimental value. Quantum corrections to H_{vap} are supposed to be small and have been neglected. The isobaric specific heat calculated as

$$c_p = \frac{\Delta E_{pot,nonb}}{\Delta T} \tag{4}$$

has a value of 140 J/(mol K). It is almost constant in the simulated temperature range. (For comparison, values for liquid benzene, 136.1; cyclohexane, 156.1, under normal conditions.)

B. Static Structural Properties. Figure 6 shows the radial distribution function (RDF) of the DPC centers of mass for three temperatures. It has relatively little structure with a main peak at 0.85 nm and almost no structure at longer distances. The small peak at 1.2 nm is an artifact due to the cutoff of the Coulombic interaction. However, there is an interesting peak

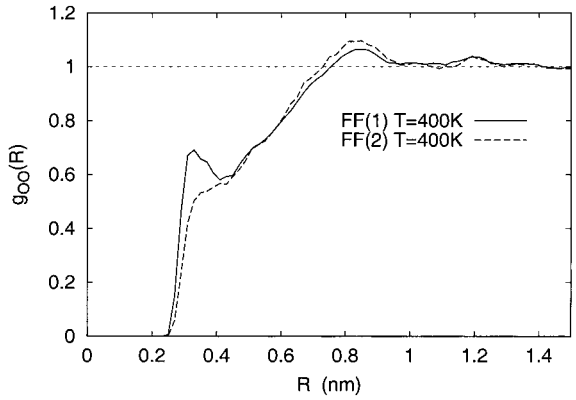

Figure 7. Radial distribution function of the central oxygen atoms in DPC at 400 K. With FF(2), the peak at 0.32 nm is slightly less favorable due to the stronger dipole of the C═O vector.

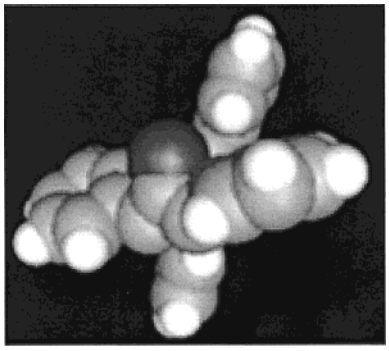

Figure 8. Crossed configuration of two neighboring molecules at small separation.

at small separation. Integration from 0 to 0.55 nm shows that this first peak is due to only one nearest neighbor. The first "complete shell" with 12 neighbor molecules is found below the main peak up to 1 nm. The temperature dependence is quite small. As one would expect, the details are smeared out at higher temperature. The peak at low separation vanishes at 573 K, leaving a shoulder at 0.6 nm.

For a better understanding of the local structure of the liquid, we discuss some more radial and orientation distribution functions. Figure 7 shows the radial distribution function of the central oxygen of the carbonate group. It exhibits a small peak at very low separation of about 0.33 nm. This peak is due to "crossed" configurations of nearest neighbors as illustrated in Figure 8. However, only about 1 out of 10 molecules has a neighbor in this configuration at 400 K. Note that, in FF(2), this small distance of the carbonate oxygens is even less favorable due to the different partial charges at the carbonate group. The crossed configurations can also be recognized in the orientation distribution function (ODF) of the "backbone vectors" $\mathbf{U}_i$ (the vector connecting the outermost carbon atoms (C_4, $C_{4'}$) of the molecule)

$$\mathrm{ODF}(R_{ij}) = \langle |\mathbf{U}_i \mathbf{U}_j| \rangle \tag{5}$$

The distance R_{ij} is measured between the midpoints of the vectors $\mathbf{U}_i$ and $\mathbf{U}_j$ which correspond approximately to the centers of mass. This ODF is equal to unity when the two vectors are parallel to each other and zero when they are orthogonal. A value of 0.5 means that the orientations are uncorrelated. Hence, Figure 9 shows that at low separation (<0.45 nm), the vectors are orthogonal to each other, indicating the crossed configurations mentioned above. However, molecules contributing to the first peak of the center-of-mass RDF at 0.5 nm prefer to be

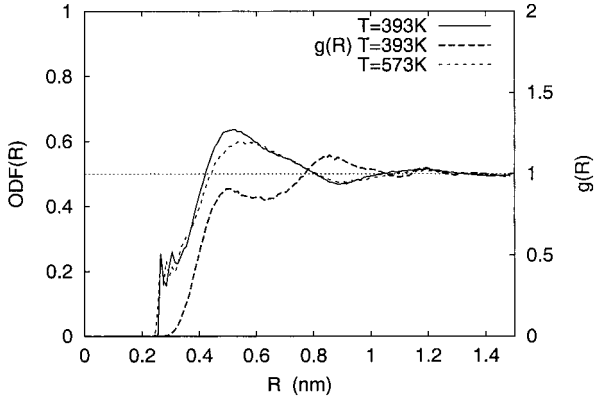

Figure 9. Orientation distribution function of the "backbone vector" as a function of distance between the centers of the molecules (1 = parallel orientation, 0 = orthogonal, 0.5 = no correlation). Also shown is the RDF (right scale) for the midpoints of these vectors which correspond almost to the center of mass.

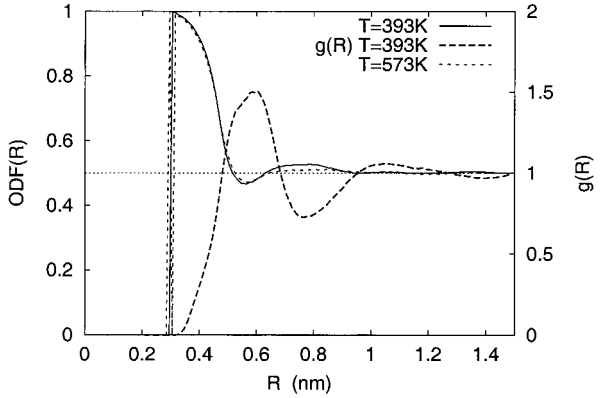

Figure 10. Orientation distribution function of phenyl ring normals on different molecules. Also shown is the RDF (right scale) of the phenyl ring centers.

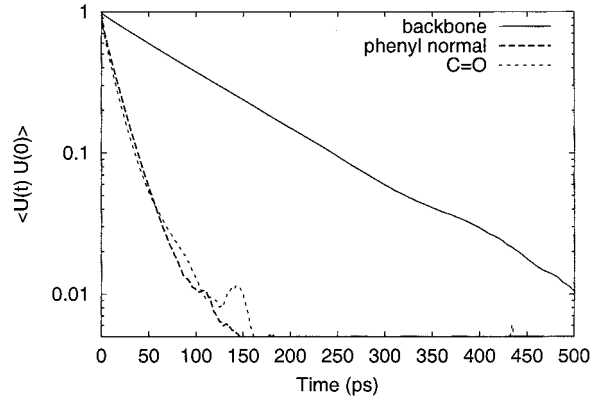

Figure 11. Orientation autocorrelation function of the cosine between backbone vectors, the phenyl normals, and the C═O vectors. Data from a trajectory of 3000 ps at 393 K.

parallel to each other. At distances of 0.85 nm, under the main peak of the center-of-mass RDF, there is a small preference for orthogonal orientation. Above 1 nm, there is no more correlation in the orientation.

Figure 10 shows the orientation distribution function of the normals of the phenyl rings on different molecules. The distance R_{ij} in this case is the distance between the centers of the phenyl rings. The figure also contains the corresponding radial distribution function of the phenyl ring centers. At very low separation, the rings must be parallel for steric reasons. However, there are very few molecules in such a position. The main peak of

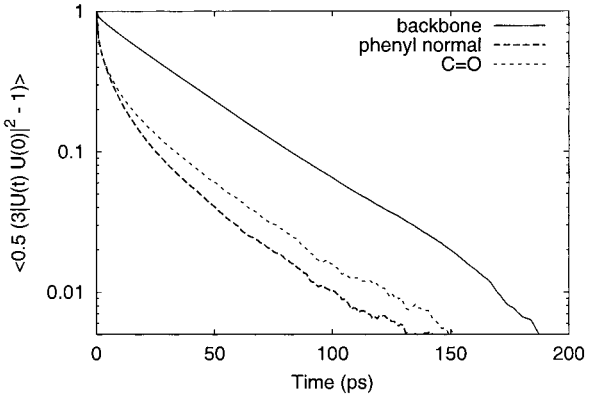

Figure 12. Orientation autocorrelation function of the second Legendre polynomial between backbone vectors, the phenyl normals, and the C═O vectors. Data from the same trajectory as preceding figure.

the radial distribution function coincides with a slight tendency to orthogonal orientation. This is similar for liquid benzene and phenol where so-called T-shaped configurations have been reported.[11]

C. Dynamic Properties. We now turn to properties such as the reorientation times of the molecules or parts of them. Figure 11 shows the time autocorrelation function of the backbone vector, the phenyl ring normals, and the C═O vector of the carbonate group

$$P_1(t) = \langle \mathbf{U}(t)\, \mathbf{U}(0) \rangle \tag{6}$$

The slowest of the three vectors to relax is the backbone vector. The relaxation of the phenyl ring normals and the C═O vector are both on the same time scale. Figure 12 shows the corresponding data for the second Legendre polynomial

$$P_2(t) = \frac{1}{2}\langle 3(\mathbf{U}(t)\, \mathbf{U}(0))^2 - 1 \rangle \tag{7}$$

which is usually more easily accessible by experiments. The figures contain the average over 3 ns at 393 K. The data at different temperatures look similar except for the time axis being scaled. To determine relaxation times, we fitted a stretched exponential to the data points:

$$f(t) = \exp(-(t/a)^{\beta}) \tag{8}$$

The relaxation time τ is then obtained by integrating $f(t)$ from zero to infinity. (For $\beta = 1$, this is just the time normalization a.) The exponents β and the relaxation times τ are summarized in Table 3 for different temperatures. The exponent β is found to be almost independent of temperature. The decay of the reorientation of the whole molecule is almost exponential (β near unity), whereas the reorientation of the phenyl ring normals and of the C═O vector are characterized by exponents of 0.7 for the cosine and 0.5 for the second Legendre polynomial. A more careful inspection shows that the stretched exponential does not yield a good description, at least for P_2 of the phenyl ring normals and the C═O vector. Their correlation functions decay very quickly at short time intervals, but they are almost parallel to the curve of the backbone vector at longer time intervals. Indeed, a better fit was obtained with a linear combination of two stretched exponentials, one with the parameters of the backbone vector and the second with $\beta = 0.5$ and a much shorter time constant a. This can be interpreted in the way that subgroups such as the C═O vector or one phenyl ring have a higher mobility than the whole molecule; they

TABLE 3: Relaxation Properties of Diphenyl Carbonate Determined from MD Simulation[a]

	T/K					
	350	393.15	400	450	500	573.15
	Reorientation					
β_{bb} (cos)	0.86	0.94	0.95	0.90	0.93	0.95
τ_{bb} (cos)	257	104	89	52	30	17.3
β_{pn} (cos)	0.78	0.78	0.80	0.81	0.81	0.83
τ_{pn} (cos)	32	15.7	14	8.4	5.6	3.5
$\beta_{C=O}$ (cos)	0.72	0.73	0.75	0.73	0.74	0.76
$\tau_{C=O}$ (cos)	29.7	14.3	12.7	7.8	5.4	3.4
β_{bb} (P_2)	0.85	0.87	0.87	0.86	0.87	0.91
τ_{bb} (P_2)	79	34	30	16.7	10.0	5.8
β_{pn} (P_2)	0.49	0.50	0.51	0.51	0.53	0.55
τ_{pn} (P_2)	21.7	9.5	8.2	4.7	2.9	1.7
$\beta_{C=O}$ (P_2)	0.46	0.47	0.47	0.47	0.50	0.53
$\tau_{C=O}$ (P_2)	28.1	12.1	10.4	5.9	3.6	2.1
	Dihedral Angle Relaxation					
$\tau(O_s-C_1)$	46.8	29.9		19.7	14.9	10.7
$\tau(O_s-C_o)$ FF(1)	4×10^5	32400	29000	6960	2090	630
$\tau(O_s-C_o)$ FF(2)			870	340		66

[a] Exponent β of stretched exponentials fitted to orientation autocorrelation functions, τ integrated relaxation times in ps. Index bb, backbone vector ($C_4-C_{4'}$); pn, phenyl ring normal; C=O, C=O vector. Mean time between flips of dihedral angles $\tau(O_s-C_1)$ and $\tau(O_s-C_o)$ in ps. Except for $\tau(O_s-C_o)$, results with FF(1) and FF(2) are very similar and only the numbers of FF(1) are given.

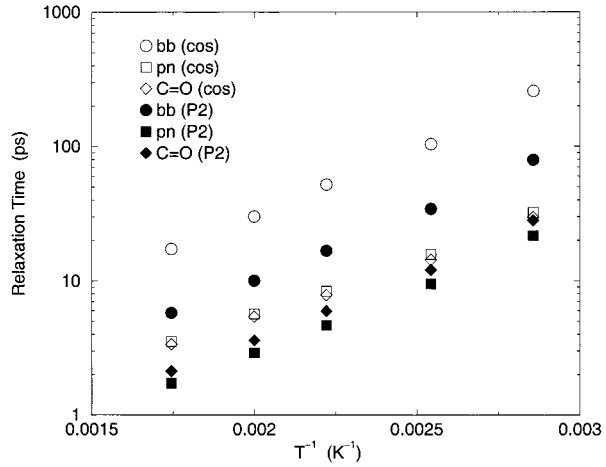

Figure 13. Arrhenius plot of relaxation times of the reorientation of the backbone vector, the phenyl normals, and the C=O vector. Open symbols = cosine; filled symbols = second Legendre polynomial P_2.

vibrate with respect to the center of mass leading to a fast short-time decorrelation. However, they are still attached to the molecule, and for longer times, their correlation decays as for the whole molecule.

Figure 13 shows an Arrhenius plot of the relaxation times. Except for the C=O vector, the first and the second Legendre polynomials yield almost the same activation energy of about 18 kJ/mol. The results for both force fields coincide within the statistical errors.

Finally, the static relative permittivity was calculated from the fluctuations of the total dipole moment of the simulation cell:

$$(\epsilon_r - 1)\left(\frac{2\epsilon_{RF} + 1}{2\epsilon_{RF} + \epsilon_r}\right) = \frac{\langle M^2\rangle - \langle M\rangle^2}{3\epsilon_0 V k_B T} \qquad (9)$$

where ϵ_0 is the vacuum permittivity and ϵ_{RF} the permittivity entering the reaction field during the simulation (3.5 in our case). Using the charges from the force field FF(1) yields $\epsilon_r \sim 1.15$ and $\epsilon_r - 1.26$ with FF(2). Using the unscaled charges of the MK-ESP fit to the charge density calculated within B3LYP and the 6-311G** basis set yields $\epsilon_r \sim 1.6$. Together with the electronic contribution of about 2 (which can be estimated from the refractive index), this is in reasonable agreement with the experimental value of 3.1 for BPA-PC. Note that the dielectric constant is quite sensitive to the relative ratio of molecules in the trans−trans and cis−trans conformations since the dipole moment of the trans−trans ground state conformation is only about 0.3 D whereas the cis−trans conformation has a dipole moment of 3.4 D (B3LYP, basis 6-311G**).

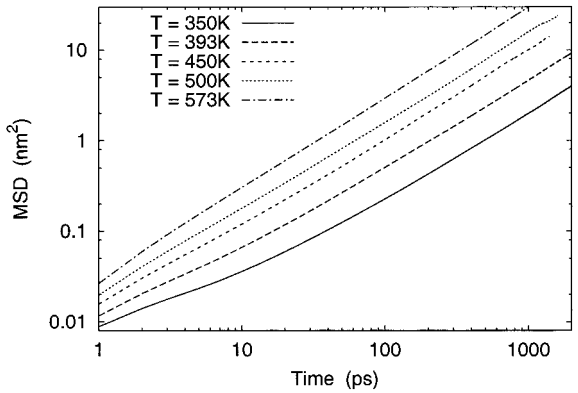

Figure 14. Mean square displacement in a double logarithmic plot. One sees anomalous diffusion at low temperatures only up to 0.1 nm^2, i.e., below half the molecular diameter.

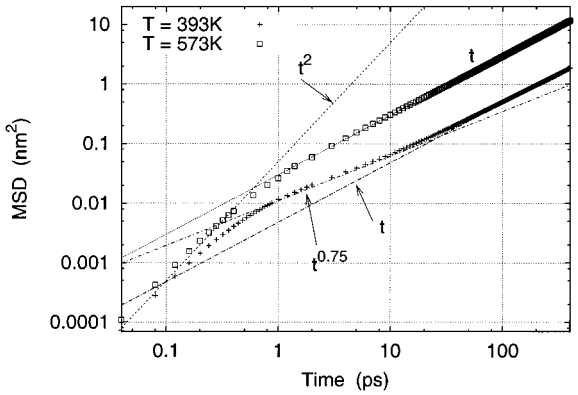

Figure 15. Mean square displacement in a double logarithmic plot. Zoom of the preceding figure with some fitting lines of the asymptotic behavior (see text).

D. Diffusion Behavior. The diffusion coefficients reported in Table 2 were determined from the mean square displacement (MSD) of the center-of-mass motion of the molecules in the normal diffusion regime. A log−log plot of this mean square displacement is shown in Figure 14. At low temperatures, an anomalous diffusion regime can be identified below 0.3 Å. At 350 K, one can speak of normal diffusion on time scales above 50 ps (MSD $\propto t^{0.6}$ below 20 ps). Above 450 K, there is no anomalous diffusion regime left. Figure 15 contains a close-up of Figure 14 with some additional data points for small time intervals. The straight lines illustrate the different diffusion regimes. A ballistic regime with exponent 2 can be identified for very small times. At high temperature, it changes directly to normal diffusion with exponent 1. At low temperature, there is an intermediate anomalous diffusion regime where the molecules are trapped in the cage of their surrounding neighbors; it is characterized in the MSD plot by an exponent smaller than 1.

An Arrhenius plot of the self-diffusion coefficient is shown in Figure 16. A linear fit to the Arrhenius plot yields an

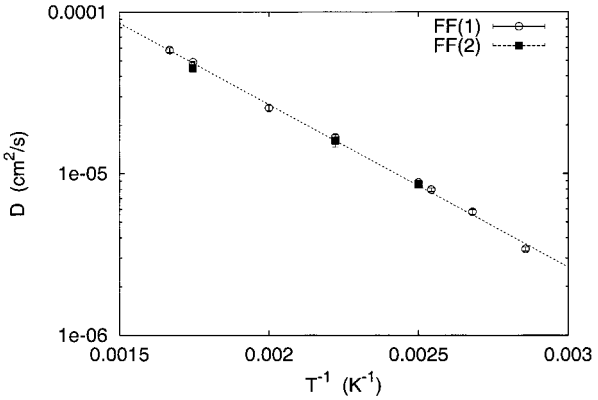

Figure 16. Arrhenius plot of diffusion coefficients for diphenyl carbonate. The dashed line represents a least-squares Arrhenius fit to the data points with FF(1) which yields $E_A = 19.2$ kJ mol^{-1}. Error bars denote the standard deviation of the three diagonal elements of the diffusion tensor (D_{xx}, D_{yy}, D_{zz}).

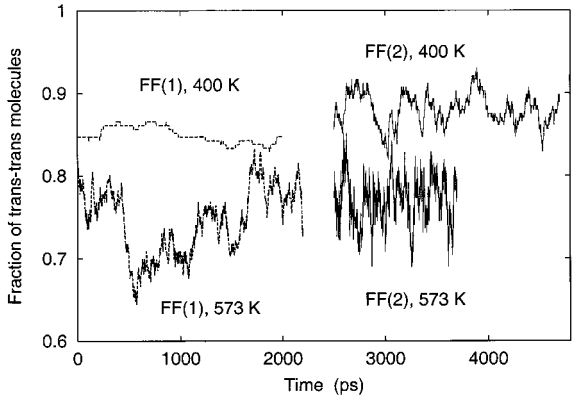

Figure 17. Evolution of the fraction of molecules in trans−trans conformation concerning the C_o-O_s bonds at low and high temperature. Dashed lines (left side), FF(1); continuous lines (right side), FF(2). Torsional angle flips are more frequent with FF(2) due to the lower torsion barrier.

activation energy of $E_A = 19.2$ kJ mol^{-1} for FF(1). With FF(2), the diffusion constant at 573 K is about 5% smaller leading to an estimate of $E_A = 18.2$ kJ mol^{-1}s. (Diffusion of DPC is about an order of magnitude slower than that of liquid phenol but the activation energy is bigger in phenol: $E_A = 25.8$ kJ mol^{-1}.[11]) The activation energy of about 19 kJ/mol for the diffusion process is of the same order as the activation energy of 18 kJ/mol for relaxation times determined in the preceding section. This suggests the picture that the diffusion process is coupled with the reorientation of the molecule and its phenyl rings.

For further discussion of the diffusion behavior, we determined effective Lennard-Jones (LJ) parameters for the DPC molecule as a whole. This is motivated by the fact that one can obtain an anomalous diffusion regime in a supercooled LJ liquid and we want to see where in the phase diagram DPC as an effective LJ liquid is situated. Calculation of the molar volume yields $\sigma_{DPC} = 0.72$ nm. Supposing six nearest neighbors, one obtains $\epsilon_{DPC} = 11.7$ kJ/mol from the intermolecular potential energy. With these parameters, the DPC melt at 393 K has a LJ density $\rho^* = 1.144$ particles per σ^3 and temperature $T^* = 0.28$. Under these conditions, a spherical LJ system is certainly crystallized under highest pressure. (A hcp lattice of hard spheres with diameter $2^{1/6}\sigma$ has a LJ density $\rho^* = 1.0$.) The same mapping performed with data of liquid phenol[11] yields $\sigma_{ph} = 0.55$ nm and $\epsilon_{ph} = 8.66$ kJ/mol. At 363 K, where the diffusion has an anomalous regime as DPC, this corresponds to $T^* = 0.35$ and $\rho^* = 1.06$. These values are intermediate between DPC and the supercooled LJ liquid at about $\rho^* = 0.89$ and $T^* = 0.55$, where we also found some anomalous diffusion. This is clear since phenol is less anisotropic than DPC and has no internal flexibility. The mapping to a sphere model might appear a crude approximation, and the determination of some effective Lennard-Jones parameters has some uncertainties, especially for ϵ, whereas the molar volume and thus σ should be quite precise. Hence, even with a factor of 2 in the temperature, the effective Lennard-Jones system would be in a frozen state. This comparison underlines that the flexibility and nonspherical form allow for the mobility of the molecules despite the high particle number density.

E. Influence of the Torsion Barrier at the Carbonate Group. The flexibility of the molecule is mainly due to rotation of the phenyl rings about the C_1-O_s bonds and to conformational flips about the O_s-C_o bonds. Figure 17 contains the evolution of the fraction of molecules having the conformation around both C_o-O_s bonds in trans orientation. (For steric reasons, only one of the two dihedrals can be in the cis orientation.) This quantity reflects directly the force field parameters leading to the torsion barrier (cf. Figure 3): The height of the barrier influences the frequency of conformational flips, whereas the energy difference between the trans−trans and the cis−trans conformations determines the mean value of trans−trans molecules plotted in Figure 17. At 400 K, about 86% of the molecules are in the more favorable trans−trans conformation versus 75% at 573 K. With FF(1) where the torsion barrier is about 40 kJ/mol, most molecules never flip such a torsion at 400 K; every step in the curve is due to exactly one flip. Note that we used a much lower torsion barrier of 13.6 kJ/mol during the equilibration run at 393 K for preparing the initial configuration of the production runs. Hence, we believe that the ratio of trans−trans and cis−trans conformations reached almost its equilibrium value. At higher temperatures, the molecule is more flexible. At 573 K, many molecules flip up to 4−10 times over 2 ns. Mean flip times $\tau(O_s-C_o)$ are reported in Table 3. (For 350 K, the estimate is very crude since only three flip events occured; at 393 K, there are already 40 events in 3 ns.) An Arrhenius fit to the flip times gives an "activation energy" of 40.4 kJ/mol. One additional remark might be interesting: the effective torsion barrier in force field FF(1) for the trans−cis flip is quite high at 40 kJ/mol. This corresponds to about 8 kT at 573 K, and one might think that such flips will never happen. However, since they occur quite often, we speculate that some collective effect helps the molecule to pass this barrier. In contrast, the rotation around the O_s-C_1 bonds is much easier as indicated by the mean flip times $\tau(O_s-C_1)$.

In FF(2), the torsion barrier at the carbonate group is much lower at about 26 kJ/mol. Hence, the mean time between conformational flips at 400 K decreases from approximately 30 ns in FF(1) to 0.87 ns in FF(2). Nevertheless, most properties are almost unchanged; especially the diffusion constant is the same within the statistical errors. This can be understood by comparing typical time scales: The mean time needed for moving about one molecular diameter, 1 nm, is 0.2 ns (see the MSD plot, Figure 14). This is still a factor of four below the mean time between conformational flips in FF(2). Hence, the carbonate torsion should have no direct effect on the diffusion. To confirm this hypothesis, we did some experiments by further decreasing the torsional potential to 20 and 12 kJ/mol. Now, the mean time between flips is 80 and 16 ps, respectively, which becomes significantly smaller than 200 ps for diffusion of 1 nm. The diffusion constant increases by 8% and 25%, respectively. For the lower torsional potential, relaxation times are between 30% (backbone vector) and 45% (C═O vector) smaller.

The density remains unchanged with the torsional potential of 20 kJ/mol; for the lower value of the torsional potential of 12 kJ/mol, the density decreases by 0.2% to the lower bound of the error bar, which should be correlated with the need for more free volume due to the frequent conformational changes.

To conclude, the behavior of the liquid is not much influenced by the height of the torsion barrier, at least above 20 kJ/mol, since the induced time scale of conformational flips is larger than the time scale relevant for diffusion. More important seems to be the energy difference between the trans−trans and the cis−trans conformations which determines the ratio between them. This influences the structure of the liquid since both conformers have different shapes. To illustrate this point, we report simulations with FF(2) where the supplementary torsion term introduced to adjust the energy difference between the conformers was omitted. In these simulations, the energy of the cis−trans conformation is only 2.2 kJ/mol higher than that of the trans−trans ground state. This leads to a fraction of trans−trans molecules of 67% at 400 K and 60% at 573 K. As a consequence, the density is almost unchanged and the heat of vaporization is decreased by about 0.4%. The largest difference is seen on the center-of-mass RDF where the peak at small separation is already washed out at 400 K.

IV. Conclusion

To summarize, we have developed and tested two all-atom force fields for diphenyl carbonate. From molecular dynamics simulations, we have evaluated the structure and dynamics of liquid DPC at a molecular level over a wide temperature range. Despite the size of the DPC molecule, its diffusion behavior is quite usual for liquids. A small anomalous diffusion regime was found for temperatures below 450 K which is explained with the closeness to the melting transition. There are indications for a coupling between conformational flexibility and diffusion properties. However, the torsion barrier at the carbonate group seems not to be a very crucial parameter, at least unless it is above 20 kJ/mol. Note that despite the very high barrier in FF-(1) torsion flips occur and should be explained with some collective effects in the dense melt. The structure and dynamics of the liquid are not so much influenced by the frequency of flips between the trans−trans and the cis−trans conformation, but more by the ratio of the two conformers since they have different shapes. It would be interesting to have experimental measurements of some dynamic quantities such as relaxation times for comparison.

Both force fields discussed in this work yield quite similar results. However, FF(1) was based on some questionable assumptions: First, the torsion barrier at the carbonate group is too large because it was calculated for dimethyl carbonate and not the whole diphenyl carbonate molecule. Second, the partial charges were adjusted to quantum calculations with basis STO-3G in FF(1) and 6-311G** in FF(2). The larger basis set should usually yield more reliable charges. However, the magnitude of the charges from STO-3G calculation turned out to be more useful in magnitude. We do not know if this is coincidental or systematic. For future use, we recommend FF-(2).

Acknowledgment. We gratefully acknowledge financial support by the Bundesministerium für Bildung und Forschung under grants BMBF-Project 03 M 4070 8 and 03 N 8008 E. We thank D. Mooney and K. Kremer for many discussions and R. Bachmann for providing experimental data.

References and Notes

(1) Polycarbonates. In *Encyclopedia of polymer science and engineering*; Mark, H. F., Kraschowitz, J. I., Eds.; Wiley: New York, 1988; Vol. 11; pp 648−718.
(2) Hahn, O.; Mooney, D. A.; Müller-Plathe, F.; Kremer, K. *J. Chem. Phys.* **1999**, *111*, 6061.
(3) Hutnik, M.; Argon, A. S.; Suter, U. W. *Macromolecules* **1991**, *24*, 5956.
(4) Sun, H.; Mumby, S. J.; Maple, J. R. *J. Am. Chem. Soc.* **1994**, *116*, 2978.
(5) Ballone, P.; Montanari, B.; Jones, R. O.; Hahn, O. *J. Phys. Chem. A* **1999**, *103*, 5387.
(6) Bendler, J. T. *Comp. Theor. Polym. Sci.* **1998**, *8*, 83.
(7) Hutnik, M.; Argon, A. S.; Suter, U. W. *Macromolecules* **1991**, *24*, 5970.
(8) Tomaselli, M.; Zehnder, M. M.; Robyr, P.; Grob-Pisano, C.; Ernst, R. R.; Suter, U. W. *Macromolecules* **1997**, *30*, 3579.
(9) Tschöp, W.; Kremer, K.; Batoulis, J.; Bürger, T.; Hahn, O. *Acta Polym.* **1998**, *49*, 61.
(10) Müller-Plathe, F. *Comput. Phys. Commun.* **1993**, *78*, 77.
(11) Mooney, D. A.; Müller-Plathe, F.; Kremer, K. *Chem. Phys. Lett.* **1998**, *294*, 135.
(12) Jorgensen, W. L.; Severance, D. L. *J. Am. Chem. Soc.* **1990**, *112*, 4768.
(13) Cornell, W. D.; et al. *J. Am. Chem. Soc.* **1995**, *117*, 5179.
(14) Singh, U. C.; Kollman, P. A. *J. Comput. Chem.* **1984**, *5*, 129.
(15) Besler, B. H.; Merz, K. M.; Kollman, P. A. *J. Comput. Chem.* **1990**, *11*, 431.
(16) King, J. A., Jr.; Bryant, G. L., Jr. *Acta Crystallogr.* **1993**, *C49*, 550.
(17) Berendsen, H. J. C.; Postma, J. P. M.; van Gunsteren, W. F.; DiNola, A.; Haak, J. R. *J. Chem. Phys.* **1984**, *81*, 3684.
(18) Ryckaert, J. P.; Cicotti, G.; Berendsen, H. J. C. *J. Comput. Chem.* **1977**, *23*, 327.
(19) Bachmann, R. Private communication.